Mechanisms of Dye Incorporation into Potassium Sulfate: Computational and Experimental Studies

Damien J. Carter,[†,‡] Mark I. Ogden,*[,†] and Andrew L. Rohl[†,§]

Department of Applied Chemistry, Nanochemistry Research Institute, Curtin University of Technology, Perth, W.A., Australia, School of Physics, The University of Sydney, Sydney, N.S.W., Australia, and iVEC, "The Hub of Advanced Computing in Western Australia", Technology Park, Kensington, W.A., Australia

Received: February 12, 2007

Potassium sulfate crystals orient and overgrow 2-aminobenzenesulfonate (OSA), and many other sulfonated aromatic compounds, on particular facets during growth from solution. The energetics associated with adsorption of OSA and benzenesulfonate (BS) were calculated using both molecular mechanical and density functional methods, in order to assess the surface binding effectiveness of these compounds on various faces of potassium sulfate. It was found that both theoretical techniques predicted that OSA and BS bind to potassium sulfate to a similar extent. The surface binding capacities were also assessed experimentally by studying the growth rates of individual faces of K_2SO_4, with results showing similar findings to those from the computational studies.

1. Introduction

The art of dyeing crystals has been pursued for around 150 years. An extensive review of the subject has been published by Kahr and Gurney.[1] Dye inclusion crystals have been investigated in the context of many areas ranging from crystal growth to solid-state lasers. Despite the wide scope of research, there is still limited understanding of the mechanism of dye inclusion.

Buckley[2,3] was the first researcher to attempt a stereochemical correlation between the host crystal structure and the functional groups on the habit modifier. He proposed that for salts of oxy anions, such as K_2SO_4, additives with anions of the form XSO_3^{n-} or XSO_4^{n-} would substitute for the salt's anions on a specific face. He suggested this would produce a change in the growth rate of the face, resulting in a change in morphology. Essentially the sulfonate−sulfate substitution mechanism will be the driving force in the formation of dye inclusion crystals. This interpretation has been used previously for studies of barite ($BaSO_4$) inhibition with organic diphosphonates.[4,5]

Although dye inclusions crystals have been studied extensively using spectroscopic techniques, the mechanism of how dye incorporation occurs is still largely unknown. Molecular modeling of organic−crystal interactions is an approach we have used with some success.[4,6−8] To date, we have published the only other computational study of the interactions of dyes with potassium sulfate surfaces.[8] Here we have used a model for dye incorporation that involves the binding of dyes to the surface as the first step. The dye can then be overgrown by the growing step fronts and eventually incorporated into the bulk crystal. We have used density functional theory (DFT) and molecular mechanical (MM) calculations, with supporting experiments, to examine this first step (surface binding), with the hope that this provides more insight into the incorporation process. We have also examined the effectiveness of the interatomic potentials used in the molecular mechanical calculations, by comparing with results from density functional calculations. Dye molecules are relatively large and complex to study computationally, so we have used two dye analogues, 2-aminobenzenesulfonate (OSA) and benzenesulfonate (BS) instead. OSA and BS were used because they have been studied extensively experimentally[9,10] and OSA in particular is known to act in a similar way to dye molecules that incorporate into potassium sulfate. This allows the computations to be less complex, while still being closely related to the systems involving more complex dyes. Also, the MM calculations can be easily extended to much larger dye systems if the DFT calculations validate the MM calculations.

2. Theoretical Calculations

Docking calculations were carried out using both molecular mechanical and density functional methods. All molecular mechanics calculations were carried out using the MARVIN[11] simulation code, with the general details of potentials used described elsewhere.[8] Atomic charges for OSA and BS were determined by fitting the electrostatic potential generated with the DFT package in SPARTAN,[12] using a DN* numerical basis set[13,14] and the Becke−Perdew[15,16] exchange-correlation functional.

Density functional docking calculations were carried out using the SIESTA code.[17,18] The generalized gradient approximation (GGA) has been employed for all calculations, using the PBE functional.[19] Core electrons have been represented by norm-conserving pseudopotentials of the form proposed by Troullier and Martins.[20] The valence electron configurations used were $1s^1$, $2s^22p^2$, $2s^22p^3$, $2s^22p^4$, $3s^23p^4$, and $3p^64s^1$ for H, C, N, O, S, and K, respectively. The 3p semicore state was explicitly included in the valence configuration of potassium to provide a more flexible and accurate description. A double-ζ basis set with polarization functions was used for all atoms except oxygen, which had a triple-ζ basis set with polarization functions. An energy shift of 0.01 Ry was used for all

* To whom correspondence should be addressed. Phone: +618 92662483. Fax: +618 92662300. E-mail: m.ogden@curtin.edu.au.
† Curtin University of Technology.
‡ The University of Sydney.
§ iVEC, "The Hub of Advanced Computing in Western Australia".

10.1021/jp071177j CCC: $37.00
Published on Web 06/08/2007

calculations. Hartree and exchange-correlation energies were evaluated on a uniform real space grid of points with a defined maximum kinetic energy of 150 Ry. SIESTA defines a *k*-grid cutoff parameter that determines the fineness of the *k*-grid used to sample the Brillouin zone.[21] A *k*-grid cutoff of 4 Å was used in all calculations, which resulted in a 2 × 1 × 2 Monkhorst−Pack *k*-grid.[22]

The bulk structure of orthorhombic β-K_2SO_4 was optimized at constant pressure (*Pmcn* space group, with $a = 5.572$ Å, $b = 10.072$ Å, and $c = 7.483$ Å[23]). The GDIS[24] program was then used to generate the (001), (010), (021), and (011) surfaces.

For surface calculations with MARVIN, a 4 × 2 surface supercell was used for the (001) and (011) surfaces, while for the (010) and (021) surfaces, a 4 × 3 supercell and a 4 × 1 surface supercell were used, respectively. The region 1 and region 2 sizes for the (001), (011), (021), and (010) surface cells were 3 and 9, 3 and 11, 6 and 13, and 2 and 7, respectively. Relaxed surfaces were generated by optimizing all atoms within region 1 (at constant volume), while all atoms within region 2 were kept fixed. The surface energy (γ) was then calculated as the difference in energy of the surface species compared to the bulk, per unit surface area:

$$\gamma(hkl) = \frac{E_{\text{surf}} - E_{\text{bulk}}}{A} \quad (1)$$

where E_{surf} is the energy of the simulation cell containing the surface, E_{bulk} is the energy of *n* equivalent number of bulk units of K_2SO_4, and *A* is the area of the surface simulation cell.

For surface calculations with SIESTA, a 2 × 1 × 3 supercell was used for the (001), (010), and (011) surfaces, while a 2 × 1 × 6 supercell was used for the (021) surface. The same *k*-grid cutoff parameter used in the bulk calculations was used in all surface calculations. As a result of the much larger cell sizes, the (010) surface was sampled with a 1 × 2 × 1 Monkhorst−Pack *k*-grid, while the (011), (001), and (021) surfaces were sampled using only the γ point. The supercells were created this way to keep the surface vectors as similar as possible, and each supercell had a vacuum gap approximately the same depth as the surface slab itself. Relaxed surfaces were generated by optimizing the surface configurations at constant volume. These calculations were then repeated using no vacuum gap, and then surface energies were calculated using the following expression:

$$\gamma(hkl) = \frac{E_{\text{slab}} - E_{\text{equivbulk}}}{2A} \quad (2)$$

where E_{slab} is the energy of the surface slab with a vacuum gap, $E_{\text{equivbulk}}$ is the energy of the surface slab with no vacuum gap, and *A* is the surface area. E_{surf} is divided by two because each slab has two equivalent surfaces. The use of $E_{\text{equivbulk}}$, rather than an integer number of E_{bulk}, allows for maximum cancellation of errors relating to sampling and convergence for the different sized simulation cells.

Docking of OSA and BS presumably involves the replacement of a SO_4^{2-} ion on the crystal surface with the $-SO_3^{2-}$ substituent. Evidence for such a mechanism, though intuitive, has accumulated.[25] A SO_4^{2-} and a K^+ ion must be removed from the surface in order to maintain charge neutrality within the simulation cell. The energy of replacing a SO_4^{2-} and a K^+ ion with OSA or BS, the replacement energy, can then be calculated:[6]

$$E_{\text{replacement}} = (E_{\text{dock}} + E_{SO_4^{2-}} + E_{K^+}) - (E_{\text{surface}} + E_{\text{dye}}) \quad (3)$$

where E_{dock} is the energy of the surface with OSA or BS contained in it and E_{K^+} and $E_{SO_4^{2-}}$ are the energies of isolated K^+ and SO_4^{2-} ions, respectively. E_{surface} is the total energy of the system containing just the relaxed surface and E_{dye} is the energy of an isolated, minimized OSA or BS molecule.

For each surface there are many combinations of SO_4^{2-} and K^+ ions that can be removed. For each symmetry independent surface SO_4^{2-}, all K^+ ions within 5 Å were considered. To avoid errors associated with interactions between periodic images, the surface areas of the simulation cells were kept as close to each other as possible. To try to ensure that the global energy minimum for the docking molecule on each surface was obtained, its orientation was varied in a number of ways above the surface (~10), for each combination of SO_4^{2-} and K^+ removed. A total of 340 different combinations were examined for OSA and BS. The fact that a number of starting positions when minimized gave the same lowest energy configuration gave confidence that the global minimum was found.

Because of the time-consuming nature of the quantum mechanical docking calculations using the SIESTA code, it was not feasible to attempt all the docking configurations that had been examined in the MARVIN molecular mechanical study. As a result, only the most stable OSA and BS orientations from the molecular mechanics calculations were used as starting positions for the quantum mechanical calculations. For each surface, up to 5 different orientations were selected for each docking molecule, which resulted in 17 quantum mechanical calculations. Optimized configurations were generated by relaxing all atoms in the simulation cell at constant volume.

3. Experimental Methods

Potassium sulfate (AR grade) was supplied by AJAX Chemicals. Potassium hydroxide (AR grade) was purchased from BDH Chemicals. Benzenesulfonic acid sodium salt (98%) and 2-aminobenzenesulfonic acid (95%) were purchased from the Aldrich Chemical Corporation.

Seed crystals were produced using a temperature-controlled bottle roller. Potassium sulfate solutions were prepared at a supersaturation (*S*) of 1.10 at 25 °C by dissolving in a 10% (v/v) ethanol−water mixture. The solution was equilibrated at 40 °C for 2 h before the temperature was ramped down at a rate of 0.2 °C/min to 25 °C and then held constant for approximately 24 h. Crystals were then filtered and washed using a saturated potassium sulfate solution. Seed crystals for growth rate experiments were individually selected under microscopic examination to ensure crystals were free of macroscopic defects and were of suitable size. X-ray powder diffraction was used to confirm the phase of seed crystals grown by this method. Growth experiments were performed using a temperature-controlled in situ growth cell suitable for optical microscopy, as described previously.[26]

Potassium sulfate solutions were prepared at a supersaturation (*S*) of 1.05 at 30 °C. The solubility at 30 °C is 12.97 g per 100 mL of water.[27] Stock solutions of OSA (4.61 g/L) and BS (4.26 g/L) were prepared which were also supersaturated ($S = 1.05$) with potassium sulfate. The OSA stock solution was prepared by adding equimolar amounts of potassium hydroxide and 2-aminobenzenesulfonic acid. Solutions were heated to dissolve the solid and then equilibrated at 30 °C. Solutions were filtered through a Gelman 0.45 μm membrane filter before use.

Seed crystals were added to the in situ cell, and the appropriate supersaturated potassium sulfate solution was pumped through the in situ cell at a rate of 1.4 mL/min. Images of crystals were captured at approximately 5 min intervals. After

TABLE 1: Calculated and Experimental Cell Parameters and Measurements of Bond Lengths and Angles of Orthorhombic β-K_2SO_4

	DFT	MM	exptl[a]
a (Å)	5.757	5.802	5.763
b (Å)	10.146	10.061	10.071
c (Å)	7.620	7.468	7.476
volume (Å^3)	445.1	435.9	433.9
S−O (Å)	1.537, 1.543	1.450, 1.459	1.459, 1.472
O−S−O (deg)	108.5, 110.2	109.2, 109.9	109.1, 110.0

[a] Results from ref 23.

TABLE 2: Surface Energies for the (001), (021), (011), and (010) Surfaces of K_2SO_4 Using DFT and MM Methods

		surface energy (J/m^2)	
face	cut	DFT	MM
(001)	0.50	0.62	0.43
(021)	0.00	0.62	0.42
(011)	0.25	0.60	0.43
(010)	0.00	0.54	0.31

30 min, 2 mL of either the OSA or BS stock solutions were added to the solution reservoir, such that the dye/salt ratio within the system was approximately 1:200, and the growth rate was measured again. For each of the additives (OSA or BS), a minimum of 20 crystals were monitored.

Crystal sizes in the (100) direction were measured over a size range of approximately 600−1500 μm, while crystal sizes in the (001) direction were measured over a size range of approximately 200−700 μm. The rates of growth of crystal faces before and after adding OSA or BS were then calculated.

4. Results and Discussion

4.1. Bulk Structure Calculations. The optimized bulk structures of β-K_2SO_4 using DFT and MM are reported in Table 1.

The calculated bulk structures of β-K_2SO_4 show close agreement to those from experimental studies. The cell volume is approximately 2.5% larger than the experimental cell, consistent with observations that GGA functionals tend to overestimate cell volumes by a few percent.[28]

Using SIESTA, we generated the band structure for the bulk structure, with the band gap calculated to be 5.8 eV. A DFT study of the band structure and optical constants by ref 29 reports the band gap as 7.9 eV. They used an augmented spherical-wave (planewave) basis set and treated exchange-correlation effects using the LDA approximation. Band gaps are very sensitive to the choice of basis set, which could explain why they report a band gap noticeably larger than the 5.8 eV from SIESTA calculations. Experimentally, the band gap has been examined using reflection spectra and has been reported as approximately 9.0−9.6 eV.[30−32] Band gaps calculated using density functional theory are systematically underestimated when compared to experimental values, and this is again the case here.

4.2. Surface Calculations. The surface energies were calculated for the (001), (021), (011), and (010) surfaces of K_2SO_4, and the results are reported in Table 2.

The surface energies from density functional calculations are approximately 1.5 times greater than the values from molecular mechanics calculations. While the absolute values from both methods are different, the trends in surface energies match very well. On visual examination of the relaxed surfaces, density functional and molecular mechanics calculations produce similar results. The relaxations of SO_4^{2-} and K^+ ions on the (001), (021), (011), and (010) surfaces were then examined. Rather than try to examine the relaxation of every atom, ions were treated essentially as a fixed group, so movements of the central sulfur atoms were measured. The displacements of atoms (in the *z* direction) have been measured by comparing the positions in the relaxed and unrelaxed surfaces. These are reported in Table 3, with a negative (−) displacement referring to inward relaxation and a positive (+) displacement referring to an outward relaxation. Visual examination of the relaxed surfaces showed each ion rotated to some degree in the *yz* plane (negligible in the *x* direction). The angles of rotation are reported in Table 4 along with the values from molecular mechanics calculations. An example of the DFT and MM relaxed surface configuration for the (001) surface is shown in Figure 1. DFT surface calculations have fewer atoms than those from MM calculations, so two cells are displayed for the DFT surface for easier comparison in Figure 1 and also in subsequent surface comparison of docking configurations. Each symmetry independent SO_4^{2-} or K^+ ion has been labeled as S1−S4 or K1−K8, respectively, for use in Tables 3 and 4 and Figure 1.

TABLE 3: Translational Relaxations (Å) of SO_4^{2-} and K^+ Ions at the (001), (021), (011), and (010) Surfaces of K_2SO_4

	(001)		(021)		(011)		(010)	
	DFT	MM	DFT	MM	DFT	MM	DFT	MM
S1	+0.08	+0.14	−0.08	+0.11	−0.09	−0.14	−0.01	−0.02
S2	−0.13	−0.08	−0.17	−0.11	+0.03	+0.06	+0.02	+0.03
S3	−0.07	−0.05	−0.03	+0.08	0.00	+0.09	−0.01	−0.03
S4	+0.07	+0.09	−0.03	−0.02	−0.03	−0.03	+0.03	+0.02
K1	−0.27	−0.17	−0.37	−0.29	−0.16	−0.07	−0.22	−0.15
K2	−0.18	−0.15	−0.28	−0.19	−0.12	−0.05	−0.07	−0.03
K3	+0.07	+0.17	−0.37	−0.20	+0.09	+0.32	−0.10	−0.01
K4	−0.05	+0.10	−0.11	+0.09	−0.26	−0.20	+0.01	−0.02
K5	−0.11	−0.11	−0.34	−0.27	−0.04	0.00	0.00	0.00
K6	+0.01	+0.03	−0.06	+0.09	−0.03	−0.11	+0.05	+0.03
K7	−0.05	−0.02	+0.09	+0.21	+0.10	+0.14	−0.02	−0.03
K8	−0.06	+0.06	−0.05	+0.12	−0.08	−0.04	+0.02	−0.01

TABLE 4: Angle of Rotation (deg) of SO_4^{2-} Ions in the *xy* Plane During Relaxation of the (001), (021), (011), and (010) Surfaces of K_2SO_4

	(001)		(021)		(011)		(010)	
	DFT	MM	DFT	MM	DFT	MM	DFT	MM
S1	27.7	27.0	3.0	3.0	1.9	2.2	2.9	5.5
S2	5.2	2.9	4.7	2.3	2.1	5.3	4.4	9.3
S3	2.8	4.4	3.6	3.6	13.6	13.5	0.9	2.0
S4	8.1	6.8	9.5	6.9	5.7	10.0	0.5	2.0

From the relaxation values reported in Table 3, the magnitude and direction of the relaxations appears to match well between the two methods. A close match is also observed for the rotational angles of the ions reported in Table 4. There are some small differences between the methods, such as the directions of the S1 and S3 ions at the (021) surface, but overall they compare extremely well. The close match between the methods indicates that the molecular mechanics potentials appear to be accurately simulating the surface structures of potassium sulfate.

4.3. Docking Calculations. Docking calculations were only performed on the (011), (001), and (010) surfaces. As a larger supercell was required for the (021) surface with DFT calculations (producing twice as many atoms as for the other surface supercells), calculations proved to be too time-consuming. The most favorable replacement energies for OSA and BS on the (001), (011), and (010) surfaces are given in Table 5.

The replacement energies from density functional calculations are approximately 1.5 times greater than the values from molecular mechanics calculations. This is consistent with the differences observed between the two methods for the absolute

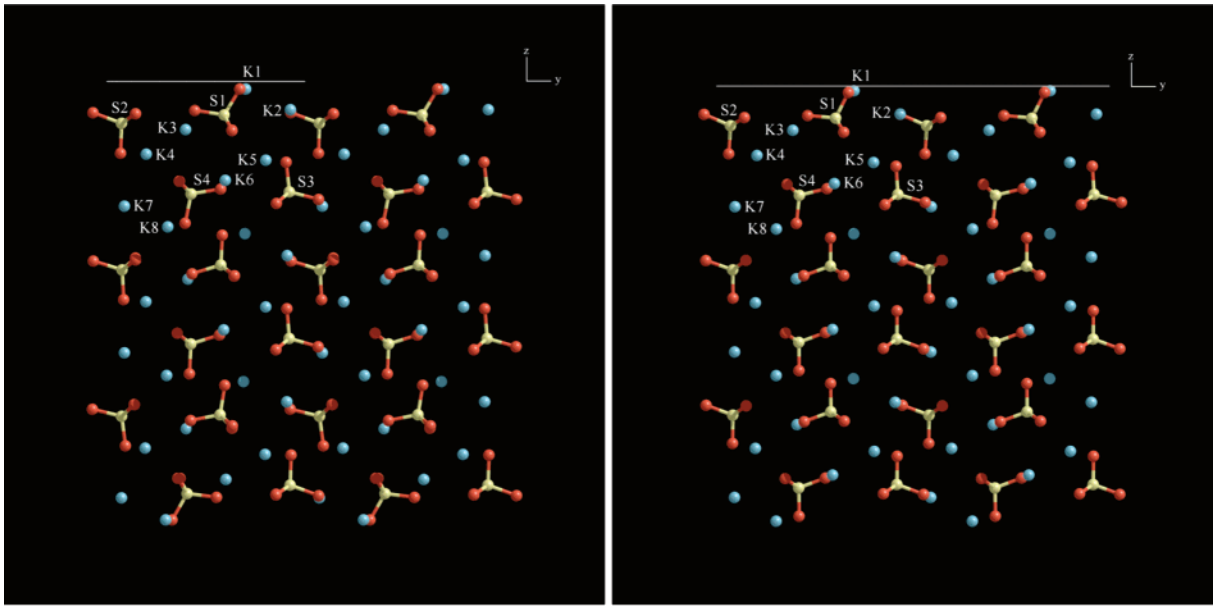

Figure 1. The calculated relaxed (001) surface of K_2SO_4 using (a) density functional theory and (b) molecular mechanics.

TABLE 5: Replacement Energies (kJ/mol) for OSA and BS Docked onto K_2SO_4 Surfaces

	DFT		MM	
face	OSA	BS	OSA	BS
(001)	1571.1	888.5	888.5	883.2
(011)	1573.4	908.9	908.9	924.8
(010)	1619.5	1025.5	1025.5	1016.9

values of the surface energies. Within each of the computational methods, the magnitudes of the replacement energies for OSA and BS are quite similar. While the absolute values are clearly different between the two methods, the relative differences between the replacement energies for each face are quite consistent. There is a small difference between the replacement energies on the (001) and (011) faces and a much larger difference between the (011) and (010) faces. The DFT derived replacement energy trend for the different surfaces from most favorable to least is (001) > (011) > (010) for both OSA and BS. The (001) surface appears to be particularly favorable for the docking of both OSA and BS, while the (010) surface appears to be quite unfavorable. This exactly matches the trends obtained from molecular mechanics calculations. In general, the surfaces do not appear to relax greatly around the docking molecules.

While the main driving force is thought to be the replacement of a surface SO_4^{2-} group with the $-SO_3^{2-}$ group of the docking

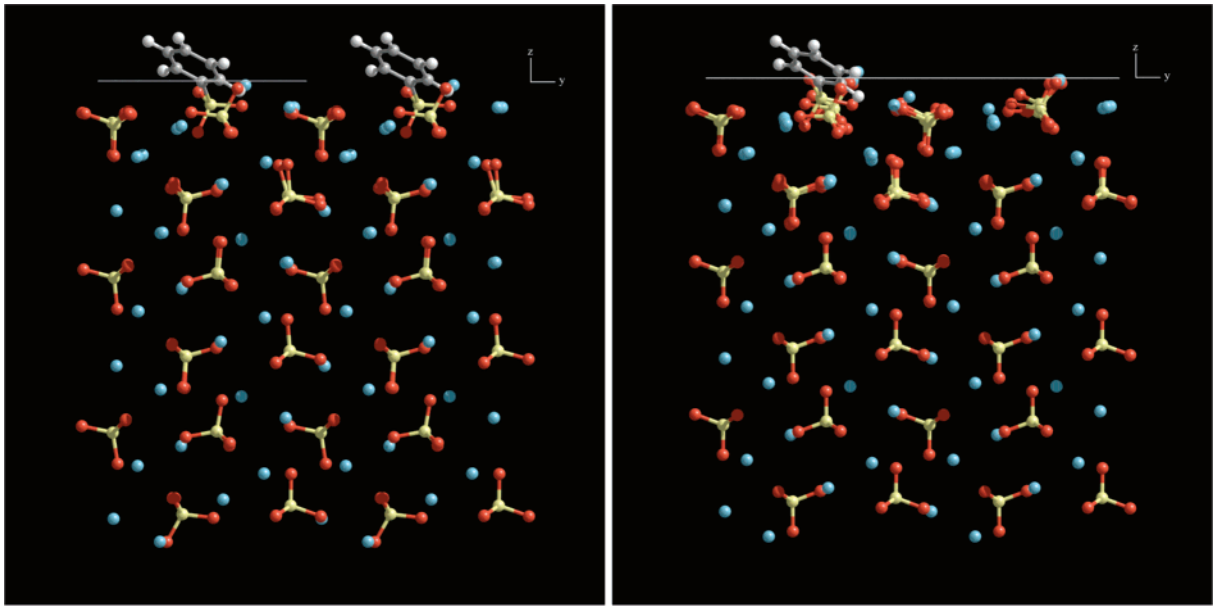

Figure 2. The most favorable BS docking configuration on the (001) surface of K_2SO_4 calculated using (a) density functional theory and (b) molecular mechanics.

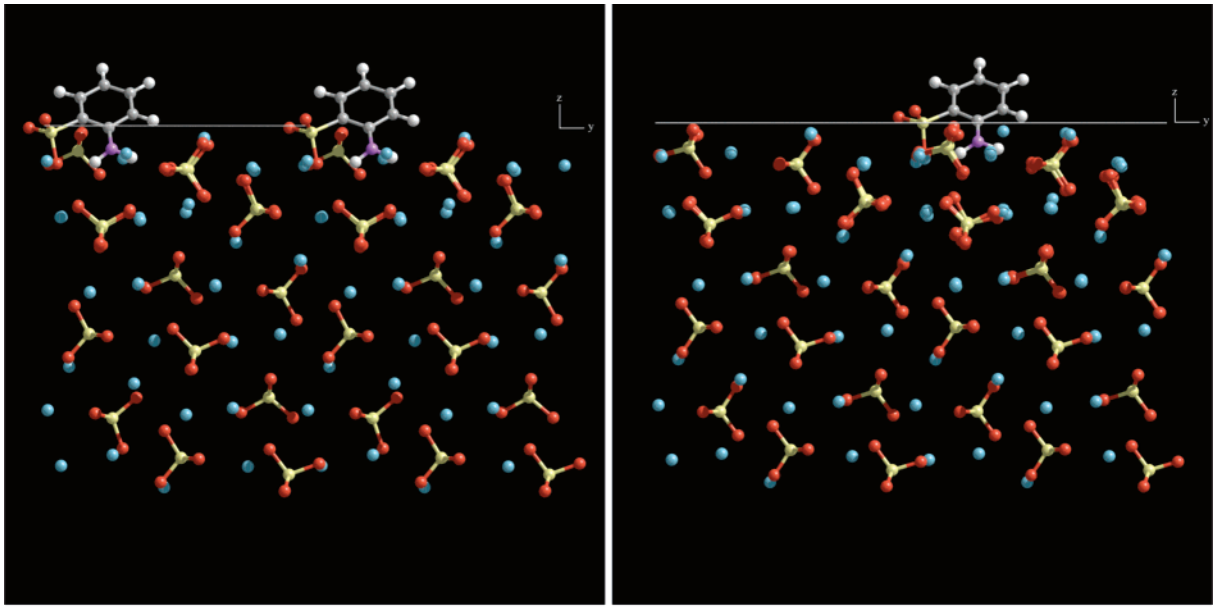

Figure 3. The most favorable OSA docking configuration on the (011) surface of K_2SO_4 calculated using (a) density functional theory and (b) molecular mechanics.

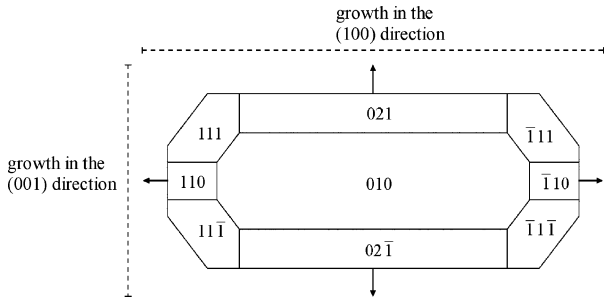

Figure 4. Growth directions of seed crystals measured during experiments.

molecule, it has also been suggested that interaction between the K^+ cations and the π-electrons of the benzene ring may have some influence.[9,25] We examined the $K^+\cdots C_6H_6$ separation for DFT and MM calculations and found close agreement, suggesting that the cation$-\pi$ interaction may have only a small influence in docking calculations or that this interaction is adequately described by the K^+ ion interacting with the negative charges centered on the carbon nuclei.

The trend in replacement energies from density functional docking calculations matches very well with results from molecular mechanics calculations. The next step is to examine and compare the most stable docking configurations from each of the computational methods. Examples of the most stable OSA and BS docking configurations using both DFT and MM are shown in Figures 2 and 3.

For each surface, DFT calculations were run on up to five different orientations of OSA and BS. In the majority of cases, the most stable OSA/BS configuration from DFT calculations matched closely with the most stable orientation from MM calculations. It is significant that in all cases, whenever the most stable orientation from MM calculations did not match the most stable orientation from DFT calculations, it matched the second most stable DFT orientation and vice versa.

Several conclusions can be drawn from these results. As both levels of computational theory predict identical docking trends for OSA and BS on the (001), (011), and (010) surfaces, this means that the interatomic potentials used in molecular mechanics calculations provide a reasonable description of the system. Gurney[10] has reported that experimentally the trend for incorporation of OSA, from most favorable to least favorable growth sector, is (001) > (011) ~ (021) > (010). Gurney[10] also reports that there is virtually no BS incorporation, with the levels of incorporation found to be approximately 48 times less than that of OSA. So while matching well with the OSA incorporation trend found experimentally, both levels of computational theory also predict that BS should incorporate to a similar extent to OSA, in contradiction with experimental findings. This suggests that surface binding of dye molecules onto terraces is too simplistic to provide a complete explanation of the incorporation process.

As mentioned before, the model used for dye incorporation involves the binding of dyes to the surface as the first step. The dye can then be overgrown by and eventually incorporated into the bulk crystal. As both DFT and MM calculations predict, OSA and BS bind to the surface of potassium sulfate to a similar extent, and we investigated this further using in situ optical microscopy.

TABLE 6: Relative Reduction in the Growth Rates of the (100) and (001) Faces of Potassium Sulfate after the Addition of OSA or BS

	growth rate (μm/s)					
	(100) face		(001) face		% reduction in growth rate	
	before	after	before	after	(100) face	(001) face
OSA	0.074 ± 0.024	0.043 ± 0.010	0.040 ± 0.008	0.018 ± 0.007	58	45
BS	0.077 ± 0.009	0.051 ± 0.006	0.027 ± 0.006	0.015 ± 0.006	66	56

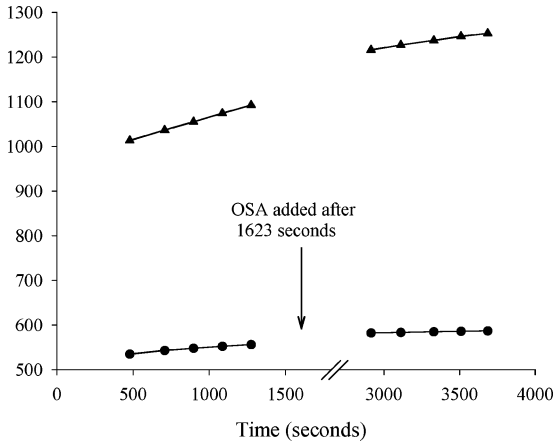

Figure 5. Example of the change in growth rates of the (100) and (001) faces of potassium sulfate after the addition of OSA (dye/salt ratio of 1:200). Data points in the (100) and (001) directions are marked with triangles and circles, respectively. Lines were fitted to data points to obtain growth rates, with all lines having correlation coefficients better than 0.98.

4.4. Growth Rate Experiments. To obtain meaningful results for the impact of additives on growth rates, they must be measured under surface integration conditions. It has been reported that at 20 °C for supersaturations (*S*) less than 1.07−1.10, surface integration is the dominant mechanism for potassium sulfate crystal growth.[33,34] These authors also reported that as the temperature increases from 20 to 50 °C, the surface integration mechanism is still dominant but the ratio of surface integration to bulk diffusion falls from approximately 75:25 to 50:50. With these results in mind, a supersaturation of 1.05 and a temperature of 30 °C were selected for use in in situ growth experiments, as these conditions should produce surface integration as the dominant mechanism. A blank run was conducted using these conditions, over the same approximate time used for additive experiments, and linear growth was observed throughout indicating that the supersaturation was not significantly depleted. Growing potassium sulfate crystals exhibit not only size-dependent growth[35−37] but also growth rate dispersion.[37,38] Hence, to simplify the growth rate measurements, the growth rates of individual crystals were examined before and after the addition of OSA and BS. By doing this, the relative change in growth rate (caused by OSA or BS) was examined, which should remove or greatly reduce the complications of size-dependent growth or growth rate dispersion. The lengths and widths of seed crystals correspond to growth in the (100) and (001) directions, respectively, as illustrated in Figure 4.

The relative reduction in the growth rates of the (100) and (001) faces after the addition of OSA or BS is summarized in Table 6. Growth rates were averaged over 10−16 measurements, and the standard deviation was used as the error measurement. A typical example of the change in the growth rates of the faces is illustrated in Figure 5.

Both OSA and BS appear to have a large effect on the growth rates of the (100) and (001) faces of potassium sulfate, with a significant reduction in the growth rates of these faces after additive addition. The influences of OSA and BS on the growth rates appear to be of comparable magnitude, albeit with large variations in both cases. From the values in Table 6, the growth rates of the (100) face in experiments is larger than that of the (001) face. This is consistent with the work of Mullin and Gaska,[39] who report that for supersaturations (*S*) less than 1.07, the growth rate of the (100) face is larger than that of the (001) face.

5. Conclusions

The calculated trend of replacement energies using both DFT and MM from most favorable to least is (001) > (011) > (010) for both OSA and BS, results that match well to experimental studies of the incorporation of OSA by Gurney.[9] However, calculations of BS replacement energies suggest that it should be incorporated similarly to OSA, in apparent contradiction to experimental findings. Thus, we also examined the effects of OSA and BS on the growth rates of individual faces of K_2SO_4 using in situ optical microscopy. A significant reduction in the growth rates of the (100) and (001) faces was observed after the addition of OSA and BS. Both OSA and BS had a similar effect on the growth rates of these faces.

Experimental and computational studies of surface binding suggest that both OSA and BS bind to the surfaces of potassium sulfate and influence the growth. Experimental studies by Gurney[9] report that BS is incorporated into potassium sulfate at a level approximately 50 times less than that of OSA. This suggests that while both OSA and BS adsorb to a surface as a first step, OSA is overgrown by subsequent growth layers and is incorporated into the bulk crystal, whereas BS desorbs from the surface rather than being overgrown. More computational studies will be required to determine what factors drive these different behaviors. As the DFT calculations have validated the accuracy of the MM calculations, we can now move forward to examine larger dyes using MM calculations with some confidence.

Acknowledgment. We would like to acknowledge the Australian Partnership for Advanced Computing (APAC) for the use of their computing facilities. We also thank J. D. Gale for his assistance with the SIESTA code.

References and Notes

(1) Kahr, B.; Gurney, R. W. *Chem. Rev.* **2001**, *101*, 893−951.
(2) Buckley, H. E. *Z. Kristallogr.* **1932**, *81*, 157−168.
(3) Buckley, H. E. *Crystal Growth*; Wiley: New York, 1951.
(4) Jones, F.; Richmond, W. R.; Rohl, A. L. *J. Phys. Chem. B* **2006**, *110*, 7414−7424.
(5) Davey, R. J.; Black, S. N.; Bromley, L. A.; Cottier, D.; Dobbs, B.; Rout, J. E. *Nature* **1991**, *353*, 549−550.
(6) Rohl, A. L.; Gay, D. H.; Davey, R. J.; Catlow, C. R. A. *J. Am. Chem. Soc.* **1996**, *118*, 642−648.
(7) Nygren, M. A.; Gay, D. H.; Catlow, C. R. A.; Wilson, M. P.; Rohl, A. L. *J. Chem. Soc., Faraday Trans.* **1998**, *94*, 3685−3693.
(8) Carter, D. J.; Rohl, A. L.; Gale, J. D.; Fogg, A. M.; Gurney, R. W.; Kahr, B. *J. Mol. Struct.* **2003**, *647*, 65−73.
(9) Gurney, R. W.; Mitchell, C. A.; Ham, S.; Bastin, L. D.; Kahr, B. *J. Phys. Chem. B* **2000**, *104*, 878−892.
(10) Gurney, R. W. Dyeing Crystals. Ph.D. Thesis, Purdue University, West Lafeyette, IN, 2000.
(11) Gay, D. H.; Rohl, A. L. *J. Chem. Soc., Faraday Trans.* **1995**, *91*, 925−936.
(12) *SPARTAN*, version 4.0; Wavefunction, Inc.: Irvine, CA, 1996.
(13) Versluis, L.; Ziegler, T. J. *J. Chem. Phys.* **1988**, *88*, 322−328.
(14) Hehre, W. J.; Lou, L. *A Guide to Density Functional Calculations in SPARTAN*; Wavefunction, Inc.: Irvine, CA, 1997.
(15) Becke, A. D. *Phys. Rev. A: At. Mol., Opt. Phys.* **1988**, *38*, 3098−3100.
(16) Becke, A. D. *J. Chem. Phys.* **1986**, *84*, 4524−4529.
(17) Ordejon, P.; Artacho, E.; Soler, J. M. *Phys. Rev. B: Condens. Matter Mater. Phys.* **1996**, *53*, R10441.
(18) Soler, J. M.; Artacho, E.; Gale, J. D.; Garcia, A.; Junquera, J.; Ordejon, P.; Sanchez-Portal, D. *J. Phys.: Condens. Matter* **2002**, *14*, 2745−2779.
(19) Perdew, J. P.; Burke, K.; Ernzerhof, M. *Phys. Rev. Lett.* **1996**, *77*, 3865−3868.
(20) Troullier, N.; Martins, J. L. *Phys. Rev. B: Condens. Matter* **1991**, *43*, 1993−2006.
(21) Moreno, J.; Soler, J. M. *Phys. Rev. B: Condens. Matter* **1992**, *45*, 13891−13898.

(22) Monkhorst, H. J.; Pack, J. D. *Phys. Rev. B: Condens. Matter* **1976**, *13*, 5188−5192.
(23) McGinnety, J. A. *Acta Crystallogr., Sect. B: Struct. Sci.* **1972**, *28*, 2845−852.
(24) Fleming, S. D.; Rohl, A. L. *Z. Kristallogr*. **2005**, *220*, 580−584.
(25) Bastin, L. D.; Kahr, B. *Tetrahedron* **2000**, *56*, 6633−6643.
(26) Lowe, J.; Ogden, M. I.; McKinnon, A.; Parkinson, G. M. *J. Cryst. Growth* **2002**, *237*−*239*, 408−413.
(27) Stephen, H.; Stephen, T. *Solubilities of Inorganic and Organic Compounds*; Pergamon Press: Oxford, U.K., 1963.
(28) Morrison, C. A.; Siddick, M. M. *Chem.—Eur. J*. **2003**, *9*, 628−634.
(29) Kityk, I. V.; Andrievskii, B. V.; Yuvshenko, V. O. *Phys. Status Solidi B* **1994**, *182*, K79−83.
(30) Plekhanov, V. G.; Osminin, V. S. *Opt. Spektrosk.* **1975**, *39*, 604−605.
(31) Plekhanov, V. G.; Osminin, V. S. *Opt. Spektrosk.* **1975**, *38*, 120−123.
(32) Andrievskii, B. V.; Kurlyak, V. Y.; Romanyuk, N. A.; Ursul, Z. M. *Opt. Spektrosk.* **1989**, *66*, 623−628.
(33) Mullin, J. W.; Gaska, C. *Can. J. Chem. Eng*. **1969**, *47*, 483−489.
(34) Jones, A. G.; Budz, J.; Mullin, J. W. *AIChE J*. **1986**, *32*, 2002−2009.
(35) White, E. T.; Bendig, L. L.; Larson, M. A. *AlChE Symp. Ser*. **1976**, *72*, 41−47.
(36) Mydlarz, J.; Jones, A. G. *Chem. Eng. Sci.* **1989**, *44*, 1391−1402.
(37) Ulrich, J.; Kruse, M.; Kallies, B.; Garside, J. *Chem. Eng. Commun.* **1991**, *99*, 25−32.
(38) Jones, A. G.; Mullin, J. W. *Chem. Eng. Sci*. **1974**, *29*, 105−118.
(39) Mullin, J. W.; Gaska, C. *J. Chem. Eng. Data* **1973**, *18*, 217−220.